Tellus (2000), 52B, 947–958
Printed in UK. All rights reserved

TELLUS
ISSN 0280–6509

Aerosol modulation of atmospheric and surface solar heating over the tropical Indian Ocean

By I. A. PODGORNY*, W. CONANT, V. RAMANATHAN and S. K. SATHEESH, *Center for Atmospheric Sciences, Scripps Institution of Oceanography, University of California, San Diego, Mail Code 0221, 9500 Gilman Drive, La Jolla, CA 92093-0221, USA*

(Manuscript received 14 December 1999; in final form 12 October 1999)

ABSTRACT

The major finding of this study is that aerosols over the tropical Indian Ocean enhance clear sky atmospheric solar heating significantly and decrease the surface solar heating by even a larger amount. The results presented here are based on aerosol chemical, microphysical, and optical and radiometric data collected at the island of Kaashidhoo (4.97°N, 73.47°E) during February and March of 1998, as part of the first field phase of the Indian Ocean experiment (INDOEX). The aerosol optical properties were integrated with a multiple scattering Monte Carlo radiative transfer model which was validated at the surface with broadband flux measurements and at the top of the atmosphere (TOA) with the clouds and earth's radiant energy system (CERES) radiation budget measurements. We consider both externally and internally mixed aerosol models with very little difference between the two models in the estimated forcing. For the February–March period, the aerosols increase the monthly mean clear sky atmospheric solar heating by about 12 W/m^2 (about 15% of the total atmospheric solar heating) and decrease the sea surface clear sky solar heating by about 16 W/m^2 with a daily range from 5 to 23 W/m^2. The net aerosol forcing at the top of the atmosphere is about -4 W/m^2 with a daily range from -2 to -6 W/m^2. Although the soot contributes only about 10% to the aerosol optical thickness, it contributes more than 50% to the aerosol induced atmospheric solar heating. The fundamental conclusion of this study is that anthropogenic aerosols over the tropical Indian Ocean are altering the clear sky radiation budget of the atmosphere and surface in a major manner.

1. Introduction

We need to quantify the radiative forcing due to both natural and anthropogenic aerosols. Currently, aerosol forcing estimates are obtained primarily from models (IPCC, 1995). Observational estimates of radiative forcing are rare (Jayaraman et al., 1998), if not non-existent. As a result, it has been very difficult to verify model results for aerosol forcing. For reasons that will be clearer shortly, it is not straightforward to obtain climatological (e.g., monthly mean) radiative forcing values directly from observations. We must resort to a hybrid approach of using aerosol-radiation models in conjunction with observations. In other words, the model input is derived from observations (e.g., aerosol chemical composition, microphysical and radiometric properties) and the model output (e.g., radiation flux) is validated with observed fluxes for a variety of meteorological and aerosol conditions. Towards this goal, we have developed an approach in this study and use this approach to estimate monthly mean aerosol forcing over the Tropical Indian Ocean. A brief description of our approach is given next.

* Corresponding author.
e-mail: igor@fiji.ucsd.edu

Our focus in this study is aerosol radiative forcing under clear skies. We need to solve this problem first before undertaking the more difficult cloud problem. The term "aerosol radiative forcing" sometimes (IPCC, 1995) refers to the effect of anthropogenic aerosols on top-of-the-atmosphere fluxes. In this paper, we adopt a more general approach, in which the aerosol radiative forcing refers to the effect of aerosols (both natural and anthropogenic) on the radiative fluxes at the top of the atmosphere (TOA) and surface. Aerosol radiative forcing, A_S, can be defined in the same way as cloud radiative forcing (Ramanathan et al., 1989):

$$A_S = S_A - S_G, \tag{1}$$

where S_A and S_G are the net short-wave radiative fluxes for a clear-sky atmosphere with and without aerosols, respectively. For a non-absorbing aerosol (e.g., sea salt), S_A is less than S_G, and A_S is negative which means that aerosol has a net radiative cooling effect. For absorbing aerosols, however, the sign of A_S would depend on relative magnitudes of absorption and scattering by aerosol, and also on surface albedo.

Unlike cloud radiative forcing, A_S is difficult to obtain directly from radiation budget observations, primarily because S_G can not be determined from observations. The atmosphere usually contains some aerosols and hence the aerosol free fluxes cannot be determined solely from the data. The strategy adopted in this study is a hybrid approach. We obtain S_G and S_A from calculated radiation fluxes using a suitable aerosol model and validate the model value of S_A with observations. If the model simulations of S_A agree with observations for a wide range of aerosol optical thickness (AOT) including small AOTs, then we are assured of the accuracy of model values for S_G (S_G approaches S_A in the limit of a vanishing AOT). At this stage, we can proceed in one of two ways: (1) use the model generated S_A and S_G to obtain A_S; or (2) use the observed S_A and model estimates of S_G to obtain A_S. In this study, we use the former approach. The input to the model is the observed AOTs and chemical composition of the aerosol.

The aerosol and radiation data used in this study were collected as part of the Indian Ocean experiment (INDOEX) first field phase (Ramanathan et al., 1996). INDOEX was designed to study the effect of anthropogenic aerosols transported from the Indian sub-continent to the tropical Indian Ocean on the regional climate. From January to April, the predominant circulation in this region consists of a low-level flow from the northeast, i.e., from the polluted land in the north to the ocean in the south. From north to south, the low level air parcels witness a transition from clear skies to marine stratocumulus to the deep-convective-cirrus cloud systems of the inter tropical convergence zone. This northeast monsoon, or alternately the Asian winter monsoon, facilitates the formation and transport of new sulfate particles, along with other pollutants (e.g., hydrocarbons) to regions of the ocean far away from urban centers. During the first field phase, data were collected from surface stations (in the Indian sub-continent, equatorial Indian Ocean and Reunion Island), ship and satellites. An important part of the INDOEX was the Kaashidhoo Climate Observatory (KCO) (4.97°N, 73.47°E) established on the island of Kaashidhoo in the Republic of Maldives. The observations at the KCO from 20 February to 31 March 1998 provided a large data set of aerosol chemical, physical and optical properties as well as radiometric surface measurements. During the experimental period, the surface winds were from the Indian sub-continent. Thus, the KCO was in a unique position to study the radiative effect of continental and anthropogenic aerosols. Prior to the first field phase, cruises have been conducted in 1996, which clearly demonstrated that sulfates and other continental aerosols are transported thousands of kilometers into the Tropical Indian Ocean with significant reduction in the solar radiation at the ocean surface (Krishnamurti et al., 1998; Jayaraman et al., 1998).

The objective of this paper is to use the INDOEX data for estimating aerosol radiative forcing over the tropical Indian Ocean. Specifically, we estimate the monthly mean clear sky aerosol radiative forcing at the surface and at the TOA and relative contribution of soot to the total forcing. Our approach of estimating aerosol forcing from equation 1 consists of the following steps.

- Develop a detailed aerosol-radiation model consistent with the aerosol chemical, microphysical and optical measurements. We have developed such a model and this is described

in detail in Satheesh et al. (1999). A summary of this model is given in the next section.

- Apply this model in conjunction with instantaneous measurements of AOT to estimate S_A at the surface and TOA and to validate those with observed fluxes. At the surface, we have observations of global and diffuse fluxes for the broadband and visible. The radiometric instruments include pyranometers, pyrheliometers and photo-diode radiometers. At the TOA, we compare the model fluxes with the clouds and earth's radiant energy system (CERES) values.
- Use the validated aerosol-radiation model in conjunction with observed daily mean AOTs to estimate monthly mean aerosol radiative forcing.

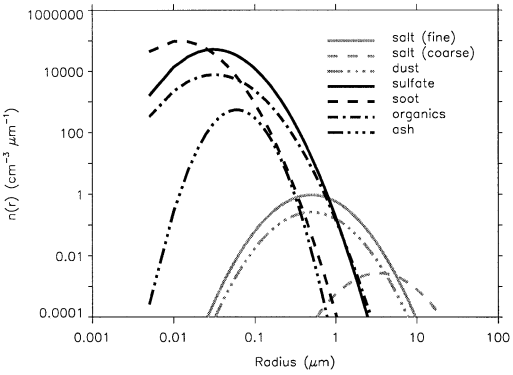

Fig. 1. The size distribution of aerosol species.

2. Description of the data and models

2.1. Aerosol model

The detailed description of the aerosol model used in this study is the subject of a companion paper by Satheesh et al. (1999). The model is constrained by the following measurements.

- AOTs at 340, 380, 440, 500, 670, 870, 940 and 1020 nm (CIMEL radiometer of the AERONET, Holben et al., 1998).
- Aerosol mass concentrations in three size ranges (<1.14 μm, 1.14–9.0 μm and >9.0 μm) for sea salt, dust, sulfate and ammonium (S/A) (three stage high volume impactor at the surface).
- Aerosol scattering coefficient at 534 nm (integrating nephelometer at the surface).
- Aerosol absorption coefficient at 565 nm (particle soot/absorption photometer at the surface).
- Aerosol vertical structure (scanning aerosol back scatter lidar, pulsed, 0.532 and 1.064 μm).

The development of the aerosol model consists of the following five steps. (1) The starting point is the standard oceanic model of Hess et al. (1998) for the size distribution of sea salt, sulfate, nitrates, ammonium and mineral dust. The size distribution of aerosol species is shown in Fig. 1. (2) The number of aerosol species in each size range is adjusted until the mass of each species agrees with the measured mass at KCO in 3 size ranges. (3) Size dependent soot aerosols are added until the surface single scattering albedo, $\bar{\omega}$, agrees with the measured values ranging from 0.88 to 0.9. (4) The columnar wavelength dependent AOT is computed next and compared with the measured AOTs. The difference between the two is negative with the magnitude of the difference being the largest in the visible. This suggests that there may be a missing aerosol component, which contains a significant sub-micron fraction. The deficit in the small aerosols is most likely due to organic aerosols (from biomass burning) which were not measured at KCO. The size distribution of the "missing organics" is inferred by adjusting the calculated AOTs to agree with the observed AOT spectral variation. (5) By examining particle filters from the particle soot absorption photometer, Prospero et al. (1998) found a gray to dark-gray coloration and suggested that the "mineral dust" component measured at KCO contains a residue of biomass burning, namely, some sort of "ash". The dust component derived from the measurements is divided into mineral dust and ash based on earlier observations of dust size distribution at Barbados by Li-Jones and Prospero (1998) (see also Satheesh et al., 1999).

Admittedly, the aerosol model includes unmeasured species such as soot, organics and ash. Of these, soot is the most important component as it dominates the surface forcing. In order to validate the aerosol model, we compare the calculated surface solar fluxes with radiometric observations and show that the calculated fluxes agree with the measurements within a few W/m^2 (Section 3). Furthermore, the calculated aerosol scattering

coefficients are well within the range of measured values (Satheesh et al., 1999).

The vertical profiles for all species are assumed to be uniform up to 1 km and then exponentially decreasing with a scale height of 800 m. This assumption is based on scanning aerosol back scatter Lidar measurements in the vicinity of the island of Kaashidhoo (Satheesh et al., 1999). The representative vertical profile of relative humidity is based on averaging the balloon sonde data obtained from the research vessel "Sagar Kanya" while in the vicinity of Kaashidhoo (Satheesh et al., 1999). As the relative humidity variations within the boundary layer are less than 10%, we use the mean profile as representative. Under cloud free conditions, relative humidity was nearly the same from 2 to 8 km. To account for vertical variations in relative humidity, we use three values: 78% from the surface up to 1 km, 62% from 1 to 2 km and 35% for altitudes above 2 km. Since sea-salt, non sea-salt sulfate and ammonium are hygrosopic in nature, different phase functions are used for the three altitude regions. While computing the broadband radiative fluxes, we use the columnar water vapor content recorded independently by the CIMEL radiometer to scale the representative profile.

Aerosol particles are assumed spherical, Mie phase function and single-scattering albedo for each aerosol species is computed using the OPAC 3.1 software (Hess et al., 1998). The input to the radiative transfer model includes a set of 10 phase functions (Fig. 2), 6 values of single-scattering albedo (Table 1), columnar AOTs and aerosol species' contributions to the columnar AOTs at different wavelengths (see Satheesh et al., 1999 for more detail). The single scattering albedo derived from the resulting model is about 0.9 at 500 nm which is consistent with the surface measurements. The model assumes that aerosol species are externally mixed. We also use internally mixed aerosol model for sensitivity studies. In this case, the volume-weighted refractive index is used for computing the phase function and aerosol single scattering albedo. As we show in the following sections, the difference between the two cases is insignificant.

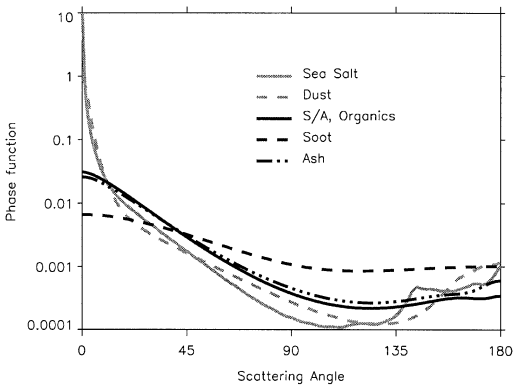

Fig. 2. Aerosol species' phase functions for the boundary layer.

Table 1. *Single-scattering albedo of aerosol species*

Aerosol type	Salt	Dust	S/A	Soot	Organics	Ash
$\bar{\omega}$	1.0	0.781	1.0	0.23	0.987	0.965

2.2. *Multiple scattering radiative transfer model*

The radiative transfer model used in this study is a clear-sky version of the Center for Clouds, chemistry and climate (C4) Monte Carlo model (Podgorny et al., 1998). The model accounts for all multiple scattering by individual aerosol species, air molecules and reflections from the surface. In the case of externally mixed aerosol, the probability of a scattering interaction with a particular aerosol species is determined by relative contribution of the species to the total aerosol extinction coefficient in a layer. Scattering angles are computed by linear interpolation in a table of the inverse cumulative scattering probability (Barkstrom, 1995), so that the model assimilates the Mie phase functions without compromising the angular resolution. We also use Henyey–Greenstein approximation to the Mie phase function as a sensitivity study. For a given wavelength, an AOT is computed by least square fitting of the spectral CIMEL optical depths in a log–log scale.

We use 2 schemes for broadband integration. The first scheme, an integration in the ultraviolet and visible (300–700 nm) at 5 nm resolution, is used for simulation of the radiometric measurements at KCO. The second scheme is applied to the entire solar spectrum (200–4000 nm) divided into 38 spectral bands and used for aerosol radiative forcing calculation.

Since the time required for a broadband Monte Carlo calculation is a linear function of the total number of photons, time expenses for calculating a monochromatic, broadband and broadband diurnal average broadband fluxes are nearly the same. A typical Monte Carlo calculation used in this study requires few seconds of the UNIX Workstation CPU time providing an accuracy of better than 1 W/m^2. The Monte Carlo model used in this study was validated by comparing with DISORT calculations.

2.3. *Description of model atmosphere and surface reflection*

The model atmosphere spans altitudes from the surface up to 100 km and has 33 reference levels. Below 25 km each layer is 1 km sick. Vertical temperature and pressure profiles are those from the US Air Force Geophysical Laboratory standard tropic atmosphere. Rayleigh scattering and ozone absorption are tabulated on the reference levels and then are linearly interpolated in the process of Monte Carlo computations using the maximum cross-section method (Marchuk et al., 1980). The extraterrestrial solar irradiance and cross sections for Rayleigh scattering and ozone absorption follow work by the World Meteorological Organization (1986). Absorption by oxygen, water vapor and carbon dioxide is calculated by exponential sum fitting using coefficients from Shi (1994).

The ocean surface albedo $\alpha_S(\mu)$ (μ is cosine of the incidence angle) is calculated according to Briegleb et al. (1986). After a reflection from the ocean, the direction of photon's motion is sampled by choosing at random between two types of reflection: Fresnel reflection from the surface and Lambertian reflection from the bulk ocean. For $\mu > 0.5$ we use Fresnel coefficient $R(\mu)$ to calculate the Lambertian component as $\alpha_S(\mu) - R(\mu)$. For $\mu < 0.5$, the Fresnel component is $\alpha_S(\mu) - 0.01$. The value of $\alpha_S(\mu)$ ranges from 0.025 for overhead sun to 0.4 for sun at the horizon, which corresponds to the wind speed of 7 m/s. The detailed surface reflection model is only important for calculating fluxes at the TOA, since the surface reflection contributes less than 1% in the global flux at the ocean surface.

We used a backward Monte Carlo model (Podgorny and Lubin, 1998) to estimate potential bias in model surface fluxes at KCO due to neglecting the perturbation of the radiation field by the reflection from the island. Kaashidhoo is a crescent shaped coral reef island about 3 km long and 1 km wide, covered by rainforest. A comparison has been made between computed surface global fluxes near the coastline and in the open ocean. We found that for clear skies the additional reflection from the island is equivalent to increasing the surface albedo by less than 0.01 and can be neglected when calculating fluxes at the surface. When calculating fluxes at the TOA, we assume the open ocean conditions.

3. Comparison of measured and calculated properties and fluxes

3.1. *Surface flux comparison*

3 instruments have been deployed at KCO for the surface measurements of global and diffuse fluxes: the Biospherical Instrument GTR-511 (400–700 nm), the Kipp and Zonen Broadband Pyranometer (300–2800 nm) and Kipp and Zonen filtered pyranometer (695–2800 nm). The fluxes in the 300–695 nm band were obtained by subtracting the filtered flux from the total flux, and will hereafter be referred to as the Kipp and Zonen filtered pyranometer measurements. The measurements of global and diffuse surface fluxes were made simultaneously by two identical (shaded and unshaded) instruments. The shading is accomplished by using a sun tracker and shadow ball arrangement. The shading ball of the sun tracker blocked the direct solar beam and 3.2° radius of the solar aureole. The flux data were screened to eliminate the effect of clouds and are believed to correspond to clear sky conditions. Each of two final collocated data sets (biospherical instrument and Kipp and Zonen filtered pyranometer) consists of 115 CIMEL, global and diffuse flux observations and represent 11% of all radiometric data collected at KCO during the INDOEX first field phase. Instrument specification, calibration procedures and data screening algorithm are described by Satheesh et al. (1999).

We used the first integration scheme (5 nm resolution) to simulate measurements of diffuse and global fluxes at the surface made with biospherical instrument and Kipp and Zonen filtered pyranometer. Whereas the comparison of meas-

ured and calculated global fluxes is straightforward, the correct comparison of diffuse fluxes requires an adjustment in the computed flux for the portion of diffuse radiation reflected by the shading ball. To remove the bias due to the shading effect, all the diffuse radiation coming to the forward cone with angular radius 3.2° was blocked out in the process of Monte Carlo simulation. We use the term "calculated diffuse flux" for the diffuse flux corrected for the shading effect.

Shown in Fig. 3 are calculated global and diffuse fluxes at the surface plotted as a function of measured flux. For the Biospherical Instrument, the measured and calculated global fluxes are in very good agreement: the mean bias is -3.8 W/m^2, root mean square (RMS) is 2.2 W/m^2, slope is 0.99, and offset at 250 W/m^2 is -1.8 W/m^2. Here mean bias stands for the average difference between calculated and measured fluxes. The slope and offset are calculated using the least square fitting. The RMS, provided as a measure of the statistical variability of the model-observation difference, is defined with respect to the residual between the model and the least-squares fitting to the observations. For the Kipp and Zonen filtered pyranometer, calculated global flux slightly overestimates the measured one when the fluxes are relatively small in magnitude (mean bias is 3.7 W/m^2, RMS is 3.3 W/m^2, slope is 0.98 and offset at 250 W/m^2 is about 7 W/m^2), but they still

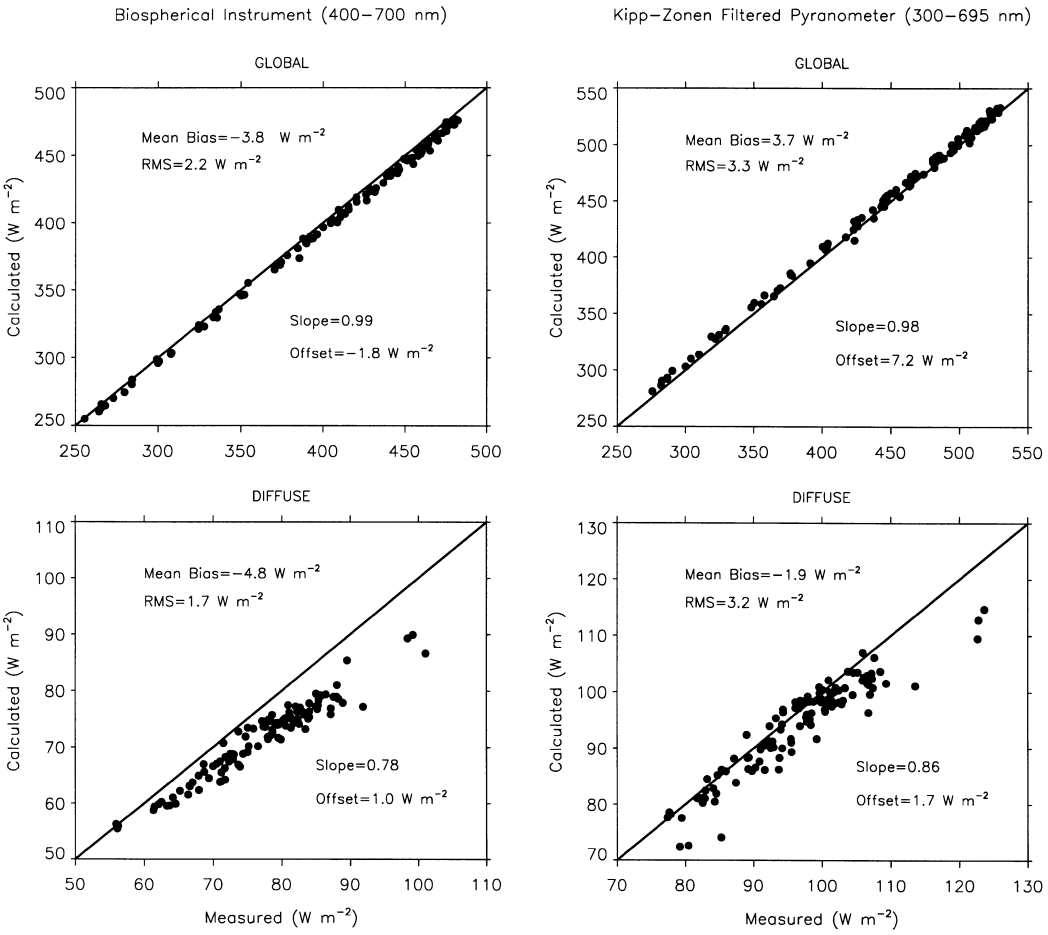

Fig. 3. Calculated global and diffuse fluxes at the surface plotted versus biospherical instrument (400–700 nm) and Kipp and Zonen filtered pyranometer (300–695 nm) measurements during the INDOEX first field phase.

agree within the measurement error limits (instrument error is 1% or approximately 5 W/m^2). For the diffuse fluxes, the agreement is better for the Kipp and Zonen filtered pyranometer (mean bias is -1.9 W/m^2, RMS is 3.2 W/m^2, slope is 0.86 and offset at 70 W/m^2 is about 2 W/m^2) compared to the biospherical instrument (mean bias is -4.8 W/m^2, RMS is 1.7 W/m^2, slope is 0.78 and offset at 50 W/m^2 is about 1 W/m^2). For the Kipp and Zonen filtered pyranometer, however, the calculated diffuse fluxes scatter over a wider range.

A potential source of the difference between calculated and measured fluxes is the uncertainty in the surface flux measurements (± 5 W/m^2). Nevertheless, there is a systematic discrepancy (Fig. 3) between the calculated and measured diffuse fluxes and the discrepancy increases with increasing fluxes (or alternately increasing AOTs). This is most likely due to the following sources:

- There is a strong positive correlation between AOT and relative humidity (Satheesh et al., 1999). The net result is that the particle size can increase (e.g., for sulfate) with AOT, which will increase the diffuse flux. This effect is ignored in our model.
- The uncertainty in phase function which was not measured at the KCO.
- The uncertainty in the treatment of the shading ball effect.

3.2. *Shading ball effect*

The comparison of calculated and measured diffuse fluxes is complicated by uncertainties due to the effect of the shading ball on the measured diffuse flux. Fig. 4 shows the calculated part of diffuse flux coming to the forward cone with angular radius 3.2°. This is the portion of the diffuse radiation blocked out during Monte Carlo simulation. Calculations are made using a set of Mie phase functions as well as Henyey–Greenstein approximations to the Mie phase functions. As seen from Fig. 4, there is a distinct disagreement between Mie and Henyey–Greenstein approaches to calculating scattering in the forward cone. By computing the forward scattered fractions for each phase function, we found that Henyey–Greenstein approximation is adequate when one needs to account for the shading ball effect for sulfate, organics and soot (relatively small particles), whereas dust and salt (relatively large particles) necessitate the use of the Mie phase function. We conclude therefore that this effect should be given more attention during the INDOEX Intensive Field Phase by performing in situ measurements of large particles size distributions in order to provide more accurate information on the phase functions of salt and dust aerosol.

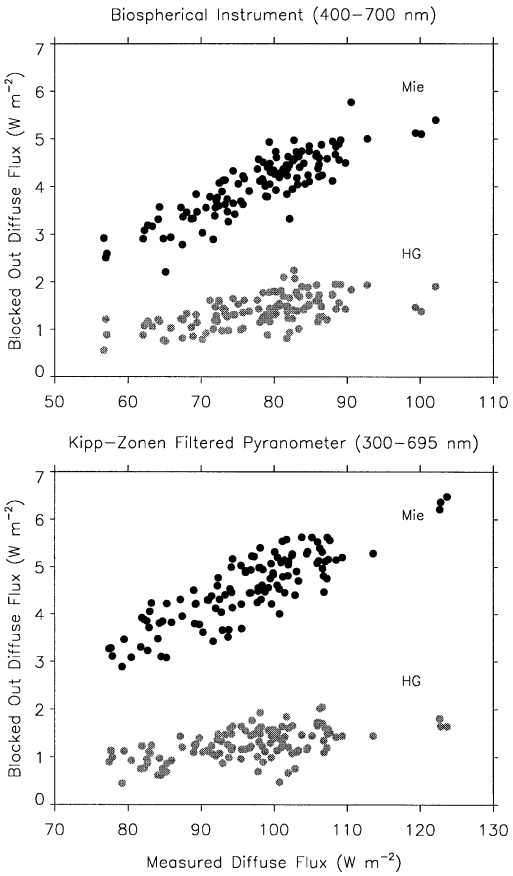

Fig. 4. Calculated diffuse flux in the forward cone with angular radius 3.2° biospherical instrument (400–700 nm) and Kipp and Zonen filtered pyranometer (300–695 nm) during the INDOEX first field phase. Calculations are made for Mie and Henyey–Greenstein (HG) approximation to Mie phase functions.

3.3. *TOA flux comparison*

In order to validate the ability of the model to accurately simulate TOA fluxes, we use CERES observations during the INDOEX first field phase. CERES was launched in December 1997 and the

data were released to the public in November 1998. The radiance measured by CERES is converted to TOA flux using an empirical algorithm (Wielicki et al., 1996) and the uncertainty of this conversion is believed to be minimum over the clear sky ocean (Ramanathan et al, 1989).

The broadband albedo of the atmosphere is computed for 24 AOTs corresponding to cloud free CERES observations at the KCO region. Fig. 5 shows comparison of collocated CERES and model broadband albedos plotted as a function of solar zenith angle. When a few data points corresponding to the solar zenith and satellite angles larger than 50° are removed, the CERES and model albedos agree within about 1% which is less than the instrumental error.

3.4. *Sensitivity of surface flux to aerosol mixing state*

As we do not have information of aerosol mixing state from in situ observations, we need to quantify the effect of mixing state on the radiative fluxes. Given that externally and internally mixed aerosol models represent two extreme cases with respect to a real mixing state, radiative fluxes computed for both aerosol models should provide a measure for the uncertainty in aerosol forcing due to lack of precise information of mixing state. Fig. 6 shows broadband fluxes at the TOA and broadband global fluxes at the surface computed for both aerosol models using the same AOTs and solar zenith angle values as for the results reported in Fig. 3. As seen from Fig. 6, fluxes for the internal aerosol model are larger at both TOA and surface, which is caused by a slight difference in single scattering albedos. The mean biases are 1.3 W/m^2 (TOA) and to 3.7 W/m^2 (surface). For February–March period, the corresponding daily mean biases are approximately 3 times less, i.e., 0.4 W/m^2 and to 1.2 W/m^2 at the TOA and surface, respectively. Thus we conclude that the difference between the internal and external models is negligible.

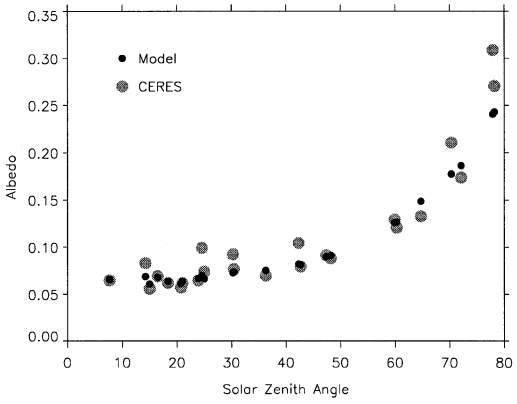

Fig. 5. Calculated broadband flux at the TOA versus CERES observations during the INDOEX first field phase.

4. Aerosol radiative forcing

Now, as we have achieved a good agreement between measured and calculated fluxes at both the surface and TOA, we apply the externally mixed aerosol model to estimate daily mean aerosol radiative forcing during the INDOEX first field phase under clear skies. We use 33 daily average AOTs derived from CIMEL measurements from 20 February to 31 March 1998, the mean AOT being 0.19. During this time period, average broadband fluxes were 306 W/m^2 at the surface and 35 W/m^2 at the TOA (322 W/m^2 and 30 W/m^2, respectively, for aerosol-free atmosphere). The aerosol radiative forcing is calculated as the difference between daily mean fluxes in aerosol and aerosol free atmospheres. Shown in Fig. 7 is the daily mean forcing at the surface and TOA as a function of Julian date in the visible broadband (400–700 nm) and broadband. The aerosol forcing shows a strong day-to-day variability, although an established long-term trend is not seen. The variability indicates the importance of synoptic scale disturbances in the Asian winter monsoon in regulating aerosol radiative forcing over the tropical Indian Ocean. It is expected that the INDOEX intensive field phase will provide observational data on day-to-day variability in aerosol composition to clarify its relationship to the variability in the atmospheric pollutant transport from the Indian sub-continent and Arabian Sea.

Fig. 8 shows daily mean aerosol forcing at the surface and TOA (the same as in Fig. 7) but now as a function of the daily mean AOT at 500 nm. Aerosol radiative forcing in the broadband has a greater variability compared to that in the visible, reflecting day-to-day variations in the column

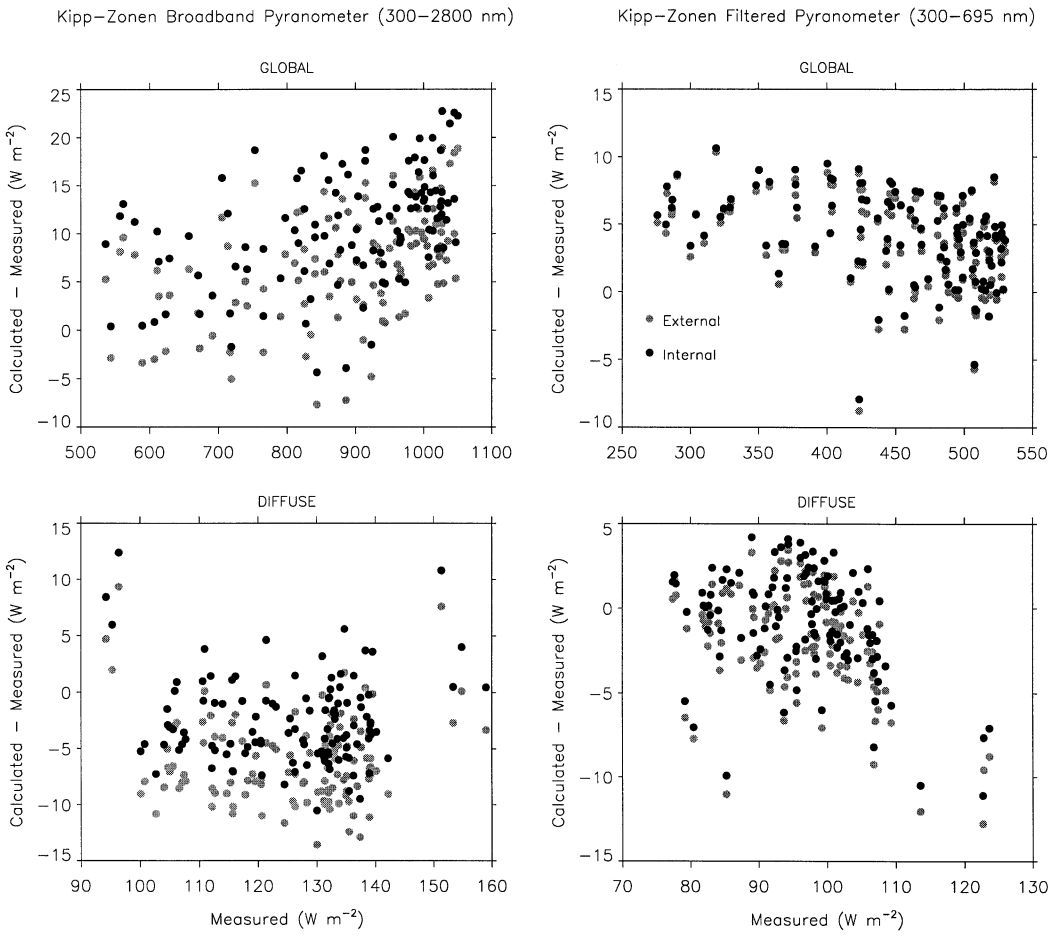

Fig. 6. The broadband fluxes at the TOA and broadband global fluxes at the surface calculated for externally and internally mixed aerosol models.

water vapor. The results presented in Fig. 8 allow an estimate of aerosol forcing efficiency defined as an absolute change in daily mean aerosol radiative forcing per unit of AOT at 500 nm. The aerosol forcing efficiency (shown in Fig. 8) is determined by least square fitting of the calculated aerosol radiative forcing to AOT. In the broadband, aerosol forcing efficiency is -20 W/m^2 at the TOA, and -82 W/m^2 at the surface.

We next focus on the aerosol atmospheric radiative forcing under clear skies, defined as the difference between aerosol forcing at the TOA and surface. The atmospheric radiative forcing is equal, therefore, to the additional absorption of solar energy in the atmospheric column due to the presence of aerosol. The aerosol-induced absorption consists of absorption by aerosol particles themselves plus additional gaseous absorption due to an increased reflection of radiation by aerosols. The aerosol forcing efficiency of the atmosphere can be found as the difference of -20 and -82 W/m^2 and equal to 62 W/m^2. Given that the mean AOT is 0.19, the average atmospheric aerosol forcing during the INDOEX first field phase is about 12 W/m^2. In the same way, we estimate the average TOA forcing to be $-20 \times 0.19 = -4$ W/m^2 and average surface forcing to be $-12-4 = -16$ W/m^2. As we have shown in previous section, the uncertainty due to lack of information on aerosol mixing state produces an

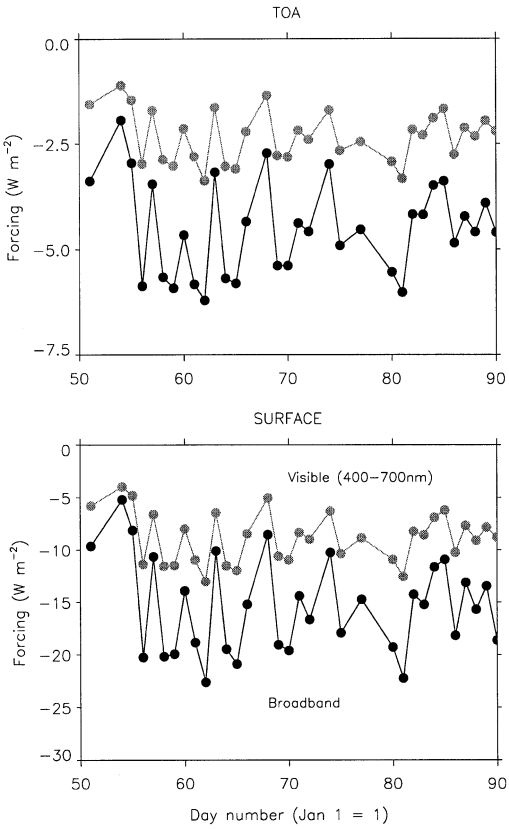

Fig. 7. Daily mean aerosol forcing at the TOA and surface during the INDOEX first field phase.

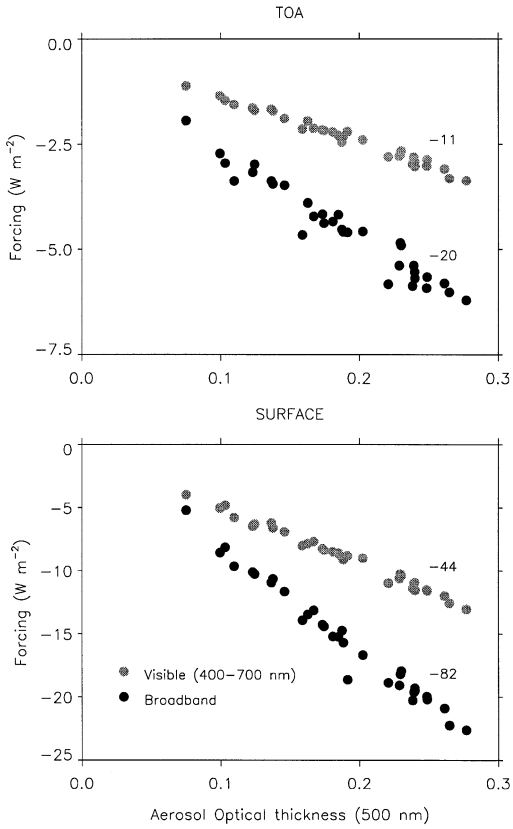

Fig. 8. Daily mean aerosol forcing at the TOA and surface during the INDOEX first field phase versus daily average AOT (500 nm).

inaccuracy being an order of magnitude less than our estimates for aerosol forcing. This means that our conclusion should be valid for both externally and internally mixed aerosol models.

Fig. 9 shows the aerosol radiative forcing for the TOA, surface and the atmosphere in the form of a bar chart. The TOA aerosol forcing is relatively small when compared to the atmospheric and surface forcing. The atmospheric forcing exceeds the TOA forcing by factor of about 3, whereas the surface forcing exceeds the TOA forcing by factor of about 4. In the case of conservatively scattering aerosol, the magnitudes of the TOA and surface forcing would be the same. The absorbing aerosol, however, decreases the TOA forcing, while changing the surface forcing to less extent. Due to the low value of single scattering albedo (Table 1), soot is the most important absorbing aerosol. The relative contribution of soot to the aerosol radiative forcing is estimated by repeating the Monte Carlo simulation for soot, while setting all other species' concentrations to zero. Aerosol radiative forcing at the TOA due to soot is slightly positive as the soot strongly absorbs radiation reflected upward from the lower layers of the atmosphere (Rayleigh scattering) and the ocean surface. Still, contribution of soot to the TOA forcing is negligible. Contrary to the TOA forcing, however, soot dominates the atmospheric aerosol forcing in both visible broadband (65%) and broadband (56%). At the surface, the aerosol forcing is also dominated by soot (43% in the visible, 35% in the broadband). Although the soot contributed only about 10% to AOT (Satheesh et al., 1999), it contributed most to the partitioning of solar

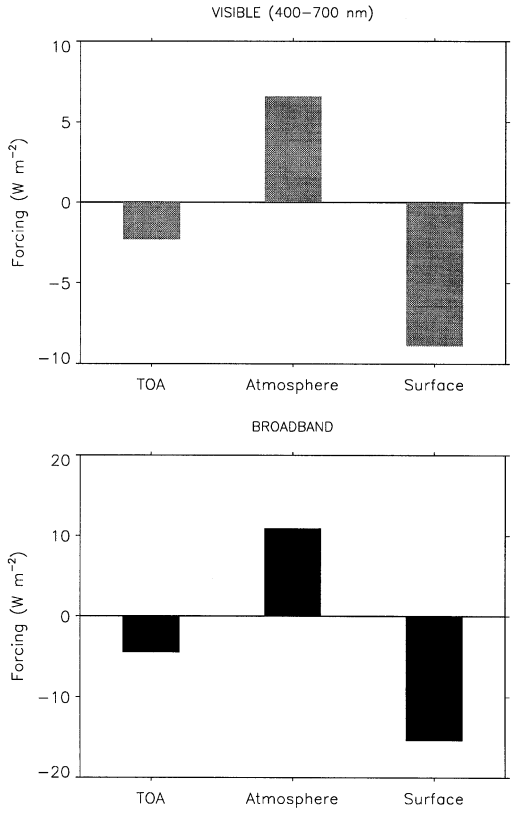

Fig. 9. Aerosol radiative forcing at the TOA, surface and in the atmosphere column during the INDOEX first field phase.

energy between the atmosphere and ocean during the INDOEX first field phase.

5. Conclusions

The aerosol model developed by Satheesh et al. (1999) and CIMEL measurements of AOT were used to calculate global and diffuse fluxes at the surface and fluxes at the TOA in the visible broadband and broadband spectral regions. The calculated surface fluxes in the visible were then compared with observations made at KCO by 3 independent radiometers during the INDOEX first field phase. The calculated and measured global fluxes in the visible are in an excellent agreement (mean bias is less than the instrumental error), whereas the calculated and measured diffuse fluxes in the visible are in a satisfactory agreement (mean bias is comparable to the instrumental error). The calculated and measured broadband global fluxes at the surface agree within 5 W/m^2 during the INDOEX first field phase (Satheesh et al., 1999). The comparison of the simulated fluxes at the TOA with CERES observations during the INDOEX first field phase also validates the aerosol model. The Monte Carlo model allows us to perform a precise comparison of measured and calculated fluxes by removing (the case of diffuse radiation) or adding (the case of direct radiation) photons entering the field-of-view of the shading ball of the instrument. The use of phase functions with high angular resolution in the direction of forward scattering is a prerequisite for a correct comparison of measured and calculated diffuse fluxes at the surface.

Both externally and internally mixed aerosol models were considered in computing the radiative fluxes at the TOA and surface. The difference in aerosol forcing caused by the lack of precise information about aerosol mixing state is an order of magnitude less that the magnitude of the aerosol forcing and hence can be neglected.

The presence of soot during the INDOEX first field phase detected earlier based on in situ measurement of aerosol single-scattering albedo was independently confirmed by a good agreement between calculated and measured surface fluxes. This finding is of great importance for understanding the atmospheric radiation budget over the tropical Indian Ocean: soot was found to dominate aerosol induced absorption in the atmosphere (more than a half of the total forcing) and the aerosol radiative forcing at the surface (about a third of the total forcing).

In absolute values, the average broadband aerosol clear sky radiative forcing during the INDOEX first field phase was -4, 12 and -16 W/m^2 at the TOA, in the atmosphere, and at the surface respectively. Because of absorption by soot and dust, the surface and atmospheric forcing are significantly larger that the TOA forcing. Thus one of the most important consequences of the aerosol pollution in the tropical Indian Ocean is the impact of the aerosol on redistribution of solar energy between the ocean and the atmosphere. The strong effect of absorbing aerosol on the radiative balance of the atmosphere is not unique for the Tropical Indian Ocean, but seems to be

common for the ocean regions affected by the anthropogenic aerosols (Hignett et al., 1999, draw a similar conclusion for the Atlantic Ocean).

6. Acknowledgements

This work was supported by the NSF Science and Technology Center for Clouds, Chemistry and Climate (C4), and this is C4 publication 208 and INDOEX publication 26. We thank A. Vogelmann for his assistance with broadband Monte Carlo model development, X. Li-Jones for her assistance with the manuscript, J. Ogren for helpful discussions and an anonymous reviewer for valuable comments on the manuscript.

REFERENCES

Barkstrom, B. 1995. An efficient algorithm for choosing scattering direction in Monte Carlo work with arbitrary phase functions. *J. Quant. Spectrosc. Radiat. Transfer* **53**, 23–38.

Briegleb, B. P., Minnis, P., Ramanathan, V. and Harrison, E. 1986. Comparison of regional clear-sky albedos inferred from observations and model computations. *J. Clim. Appl. Meteor.* **25**, 214–226.

Hess, M., Koepke, P. and Schult, I. 1998. Optical properties of aerosols and clouds: the software package OPAC. *Bull. Am. Met. Soc.* **79**, 831–844.

Hignett, P., Taylor, J. P., Francis, P. N. and Glew, M. D. 1999. Comparison of observed and modeled direct aerosol forcing during TARFOX. *J. Geophys. Res.* **104**, 2279–2287.

Holben, B. N., Eck, T. F., Slutsker, I., Tanre, D., Buis, J. P., Setzer, A., Vermote, E., Reagan, J. A., Kaufman, Y. J., Nakajima, T., Lavenu, F., Jankowiak, I. and Smirnov, A. 1998. AERONET — A federated instrument network and data archive for aerosol characterization. *Remote Sens. Environ.* **66**, 1–16.

IPCC: *Climate change, the IPCC scientific assessment*, 1995. Cambridge University Press.

Jayaraman, A., Lubin, D., Ramachandran, S., Ramanathan, V., Woodbridge, E., Collins, W. and Zalpuri, K. S. 1998. Direct observations of aerosol radiative forcing over the tropical Indian Ocean during the Jan.–Feb. 1996 pre-INDOEX cruise. *J. Geophys. Res.* **103**, 13,827–13,836.

Krishnamurti, T. N., Jha, B., Prospero, J. M., Jayaraman, A. and Ramanathan V. 1998. Aerosol and pollutant transport over the tropical Indian Ocean during the 1996 northeast monsoon and the impact on radiative forcing. *Tellus* **50B**, 521–542.

Li-Jones, X. and Prospero, J. M. 1998. Variations in the size distribution of non sea-salt aerosols in the marine boundary layer at Barbados: impact of African dust. *J. Geophys. Res.* **103**, 16,073–16,084.

Marchuk, G. I., Mikhailov, G. A., Nazaraliev, M. A., Darbinjan, R. A., Kargin, B. A. and Elepov, B. S. 1980. *The Monte Carlo methods in atmospheric optics.* (Springer Ser. in Opt. Sci., vol. 12.) Springer-Verlag, New York.

Podgorny, I. A. and Lubin, D. 1998. Biologically active insolation over Antarctic waters: effect of highly reflecting coastline. *J. Geophys. Res.* **103**, 2919–2928.

Podgorny, I. A., Vogelmann, A. M. and Ramanathan, V. 1998. Effects of cloud shape and water vapor distribution on solar absorption in the near infrared. *Geophys. Res. Lett.* **25**, 1899–1902.

Prospero, J. M., Maring, H. and Savoie, D. Aerosol chemical composition, light scattering and light absorption in the Maldive islands during the Indian Ocean winter monsoon: the impact of continental sources on aerosol radiative properties. *INDOEX Workshop Meeting Notes*, Utrecht, The Netherlands, 20–28 June 1998. INDOEX International Project Office, La Jolla, USA, 1998.

Ramanathan, V., Cess, R. D., Harrison, E. F., Minnis, P., Barkstrom, B. R., Ahmad, E. and Hartmann, D. 1989. Cloud–radiative forcing and climate: results from the earth radiation budget experiment. *Science* **243**, 57–63.

Ramanathan, V., Crutzen, P. J., Coakley, J. A., Clarke, A., Collins, W. D., Dickerson, R., Fahey, D., Gandrud, B., Heymsfield, A., Kiehl, J. T., Kuettner, J., Krishnamurti, T., Lubin, D., Maring, H., Ogren, J., Prospero, J., Rasch, P. J., Savoie, D., Shaw, G., Tuck, A., Valero, F. P., Woodbridge, E. L. and Zhang, G. 1996. *Indian Ocean experiment (INDOEX).* C4 Report. Scripps Institution of Oceanography, UCSD, La Jolla, USA (this report is available at the website: HYPERLINK http://www-c4.ucsd.edu) @http://www-c4.ucsd.edu).

Satheesh, S. K., Ramanathan, V., Li-Jones, X., Lobert, J. M., Podgorny, I. A., Prospero, J. M., Holben, B. N. and Loeb, N. G. 1999. A model for the natural and antropogenic aerosols over the tropical Indian Ocean from INDOEX data. *J. Geophys. Res.* **104**, 27,421–27,440.

Shi, L. 1994. Cloud radiative forcing on surface shortwave fluxes: a case study based on cloud lidar and radar exploratory test. *J. Geophys. Res.* **99**, 25,909–25,919.

Wielicki, B. A., Barkstrom, B. R., Harrison, E. F., Lee III, R. B., Smith, G. L. and Cooper, J. E. 1996. Clouds and the earth radiant energy system (CERES). An earth observing system experiment. *Bull. Am. Met. Soc.* **77**, 853–868.

World Meteorological Organization, Atmospheric ozone. 1986. *WMO Report* **16**, 355–362 (Geneva).